Square Wave Optimization in Vertical-Cavity Surface-Emitting Lasers Subjected to Polarization-Rotated Optical Feedback

by

Taylor Wade Gilfillan

An Honors Thesis

Presented to

The Faculty of the Department of Physics and Engineering

Washington and Lee University

in partial fulfillment of the requirements for the

Degree of Bachelor of Science

12 April 2013

_____

Dr. David W. Sukow, Supervisor

Abstract

I experimentally study the dynamics of vertical-cavity surface-emitting lasers (VCSELs) with polarization-rotated optical feedback. This type of semiconductor laser naturally emits linearly-polarized light and can elicit complex laser dynamics when subjected to optical feedback. Polarization-rotated optical feedback is created by a mirror placed a distance away from the laser (forming an external cavity) and the rotation of the feedback's polarization by 90° while in the cavity before being reinjected into the laser. Among the various complex dynamics that can possibly result from this form of feedback include chaotic behavior, polarization mono- and bistability, and square-waves. My experimental studies focus on the regularity of these square-waves. Noisy, square-wave-like polarization switchings are observed with periodicity slightly longer than twice the cavity round-trip delay time. I perform a separate parameter space study that indicates optimum operating conditions exist in feedback strength and pump current, for which the square waves are most regular. This conclusion is supported by careful examination of time series data, as well as statistical studies of the mean switching period.

Following my experimental results, I present the mathematical model used to numerically simulate a VCSEL known as the spin-flip model. This model specifically accounts for the rotated feedback present in our system and provides numerical results that further support our conclusion for square-wave optimization via mapping parameter space for pump current and birefringence of the semiconductor material.

Table of Contents

I. Introduction

A. Semiconductor Lasers

i. Brief History

Since their development in 1962, Semiconductor lasers (SLs) have taken on a huge role in scientific research and technology, revolutionizing optical science and fostering a number of subfields within the discipline [1]. The world increasingly relies on the products of laser technology, ranging from high-speed telecommunication networks to barcode scanners at your local store. As the reader may know, the acronym "laser" stands for light amplification by stimulated emission of radiation. The two universal components all lasers share is a medium that provides light amplification through means of stimulated emission, and a cavity which acts as a feedback mechanism and frequency selector.

Einstein was the first to postulate the idea of stimulated emission in 1917, an idea that he arrived at following his understanding of spontaneous emission of free atoms [2]. In his 1917 paper, Einstein describes spontaneous emission as the inevitable transitioning of an atom from an excited state to a lower state via the release of energy in the form of a photon. Artificially inducing this process by bombarding excited atoms with photons of the appropriate frequency is known as stimulated emission. This process is detailed at the top of the following page (Fig. 1.1), which walks through the steps of producing stimulated emission. Thus, a laser utilizes a particular gain medium leading to spontaneous emission that, when coupled with the correct cavity length, provides the appropriate frequency of light need to amplify light by stimulated emission.

A number of different gain media have proven to be effective in the process of lasing, including gas, dye and solid-state lasers. The type of gain media we draw our attention to are

semiconductors. The photonics industry was originally focused on a type of semiconductor laser known as an EEL (edge-emitting laser), a useable laser diode for technology but one that possesses certain downsides. Non-ideal properties of EELs include a non-circular

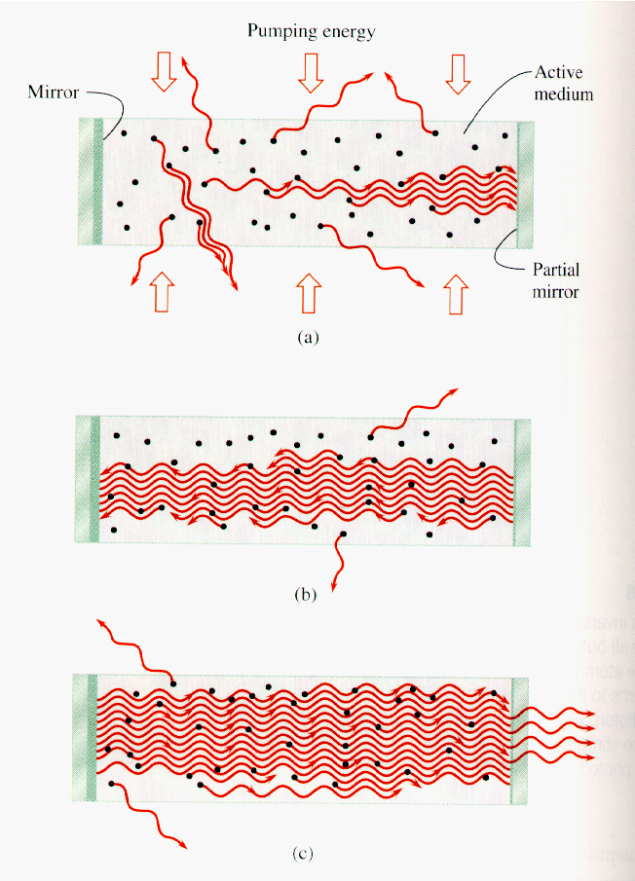

Figure 1.1 The process of stimulated emission resulting in lasing action. As electrical current triggers spontaneous in (a), some is light is scattered away but some begins to propagate in the same direction. In (b), we see a stronger coherent light beam forming, resonating between the two mirrors. The reflected photons are likely to stimulate emission from surrounding atoms. By (c), the laser has reached a steady state and produces a steady beam of light. In every diagram here, light is escaping the external cavity, but we show the light exiting in c) to indicate the laser has thermalized. Figure reproduced from [3].

aperture, high degree of beam divergence, and their inability to be tested during the manufacturing process which increases production costs [4]. In 1989 a new type of continuous-wave SL was brought into existence: the vertical-cavity surface-emitting laser (VCSEL) [4]. In the next subsection I discuss the structure and properties of VCSELs, highlighting specific characteristics that are desirable.

ii. VCSELs

Before going into detail about VCSELs, I would like to give a brief overview of the general process of how they lase. All semiconductor lasers produce coherent light by means of passing electrical current through their gain medium, which produces electron-hole pairs (described in next paragraph) in the semiconductor. The gain medium, also known as the active layer, consists of this semiconductor material which has electrical current pumped through it. Once the electron-hole pairs are recombined, photons are produced in the form of stimulated emission.

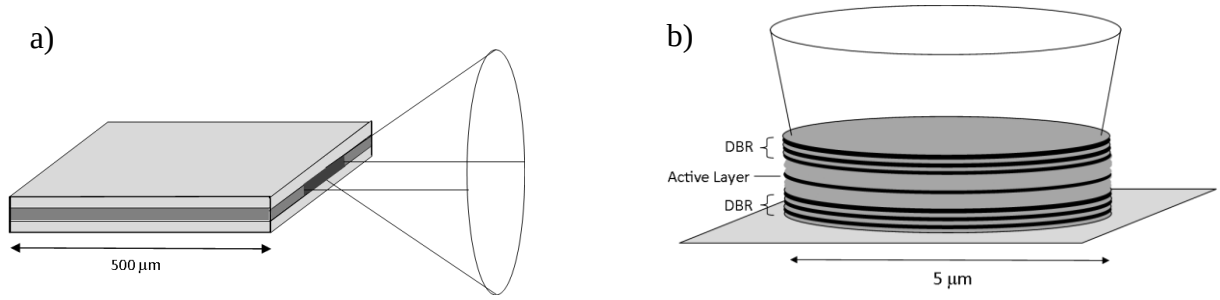

Figure 1.2 Basic structures of a) Edge-Emitting Laser (EEL) and b) Vertical-Cavity Surface-Emitting Laser (VCSEL). Note the EEL has a more divergent, elliptical beam while the VCSEL produces a circular, less divergent beam. Also, the EEL's cavity is oriented parallel to the wafer surface, while the VCSEL's cavity is perpendicular to its surface. In terms of production materials and costs, note the efficiency of the VCSEL's size: its surface is orders of magnitude smaller than an EEL yet produces an often advantageous beam profile. The VCSEL structure is described in greater detail in the main text.

Shown in Fig. 1.2, one of the main structural differences between EELs and VCSELs is rooted in their names: EELs emit light horizontally out of their structure (parallel to its active layer), while VCSELs are designed to release light vertically (perpendicular to its active layer). These two semiconductor lasers vary in many other ways, but I will focus on describing the VCSEL alone.

Let us begin by taking a closer look at the active layer, beginning with the formation of electron-hole pairs and population inversion. Consider a single atom in the gain medium with a

finite number of electrons in the ground state. After being bombarded with photons of the appropriate frequency, some of those electrons with transition to an excited state, leaving "holes" in the ground state shell that are empty: this is the essence electron-hole pair formation (Fig. 1.3). I present this concept in a simplified manner, as "holes" in semiconductor physics hold a deeper meaning and this explanation suffices for the matter at hand.

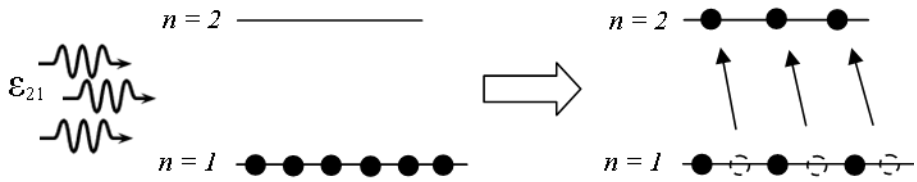

Figure 1.3 Simplified representation of electron-hole pair formation between a ground state ($n = 1$) and an excited state ($n = 2$). The atom absorbs the three photons (on left), which excites three electrons to the n=2 state. This is a basic model of a process that can involve multiple excited states and transitions to achieve a larger inverse population.

Expanding our view to the bulk of the semiconductor material, we can talk about the existence of electron-hole pairs across a large sample of atoms in what are called energy bands, which are described by their total angular momentum J. There are two energy bands (conduction and valence) in VCSELs between which two transitions are allowed: the transition between $J_z = -1/2$ to $J_z = -3/2$, and from $J_z = 1/2$ to $J_z = 3/2$ (Fig. 1.4). We say that an inverse population forms in the active layer when more electrons are present at the higher energy level (conduction band) than at the lower energy level (valence band) [5]. To produce the most power from our laser in the form of coherent light, we maximize the number of electron hole pairs formed at a given instant, usually by means of increasing the electrical pump current sent through the active layer.

To arrive at a better understanding of the full VCSEL picture, we first acclimate ourselves

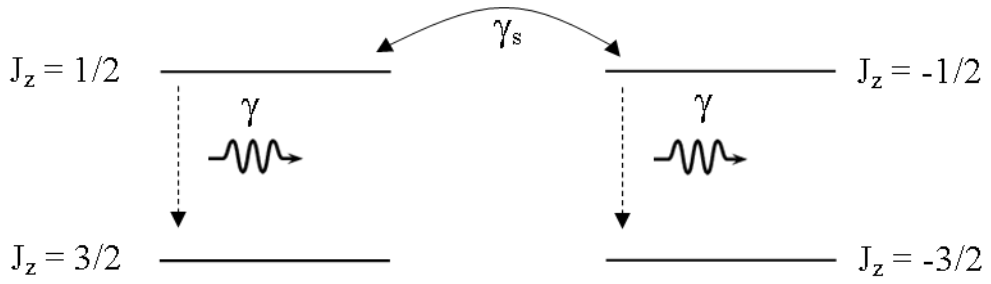

Figure 1.4 A model displaying the two electron transitions available in a VCSEL's active layer. While the two transitions involve $\Delta J_z = \pm 1$, two separate carrier populations are present. The importance of this will be discussed in section III when we mathematically model the VCSEL's dynamics.

to a different structural feature of the VCSEL. A clever arrangement of layered materials on top and bottom of the active layer form devices known as distributed Bragg reflectors (DBRs) which utilize their indices of refraction and spacing to create highly reflective coatings, providing over 99% reflectance. For VSCELs, the DBRs are perpendicular to the direction of transmission of light, which we know already know travels vertically through the structure. These DBRs provide the necessary light amplification by resonating stimulated emissions within the active layer, letting a small portion of light escape through one layer of the DBR which has a slightly lower reflectance rating than the other; this process was shown illustratively in Fig. 1.1 earlier.

What results from the sandwiching of the active layer between DBRs is the basic structure of a VCSEL. Among the appealing characteristics of a VCSEL are its circular beam profile (divergence of 10°-20°, ideal for coupling with circular optical fibers [5]), simplicity of device testing during production, low power consumption, and easily controllable polarization. VCSELs are nowadays widely employed in photonics applications as they have many advantages as compared to EELs, which are generally more powerful but have certain manufacturing and operational downsides.

B. Time-Delay Systems

Delayed optical feedback arises unavoidably in laser technology ranging from fiber optics to data storage. As the technology was being developed, scientists needed to account for complex issues arising from delayed feedback in their laser systems. What started as a revising of technological designs to account for delayed feedback developed into the study of optical feedback at a fundamental level. Looking at semiconductor lasers, one of their particularly interesting characteristics is their ever-growing range of possible dynamic outputs when subjected to optical feedback. Creating feedback in a laser system can be as simple as reflecting the output light of the laser back into it using a high-reflectivity mirror: this type of configuration is called a time-delay system.

Time-delay systems can be mathematically described using delay differential equations (DDEs), which are coupled rate equations whose solutions necessitate having information about a system at some delayed rate of time τ. DDEs are used in a wide spectrum of applications in numerous fields such as car-following models, fluid dynamics, and modeling combustion engines [6]. We say a DDE solution requires an infinite-dimensional set of initial conditions from $t = -\tau$ to $t = 0$. This means that if there is a time lag τ in a system, we need to know the solution profile over an interval that is equal to τ in order to produce a full solution. Compare this scenario to time-dependent solutions of ordinary different equations (ODEs). For a first-order linear ODE, a solution calls for a single initial value at a given time t. Consider the initial value problem

$$\frac{dy}{dt} = ky,\ y(0) = 1 \tag{1.1}$$

which maps the exponential solution

$$y(t) = \mathrm{e}^{kt} \tag{1.2}$$

At any time *t*, you can know the exact value of $y(t)$ without having to know where it was previously. This is not the case with DDEs, where a similar case expresses itself as

$$\frac{dy}{dt} = ky(t-\tau),\ y(t) = 1 \text{ when } -\tau \leq t < 0 \tag{1.3}$$

where we see the right hand side now has a function of $y(t-\tau)$ and we are provided with an initial *function* given over a finite time interval instead of an initial value. This is why DDEs are formally known as infinite-dimensional: they require a continuum of initial conditions.

C. Square Waves

i. Polarization-Rotated Optical Feedback

The study of optical feedback-induced phenomena in semiconductor lasers attracts much attention, motivated, on one hand, by the many applications of external-cavity SLs and, on the other hand, from a nonlinear science point of view for the rich variety of complex behaviors that are induced by the time-delayed feedback [7–10]. Conventionally, optical feedback has been studied in systems that involve taking a laser beam travelling through an external cavity and reflecting it back at the laser. An optical feedback scheme of particular interest has been referred to as polarization-rotated (PR) feedback or orthogonal feedback [11–19]. In this scheme a 90° polarization-rotating device is placed in the external cavity, and thus, the associated linear orthogonal polarizations (in the following referred to as *x* and *y*) are mutually fed back: *x*-polarized light is reinjected into the laser as *y*-polarized light after a delay time *τ*, and vice versa. Since these systems experience delayed feedback, they necessitate the use of DDEs to model their dynamical behavior; I will cover this modeling in section III. More importantly is that this

feedback scheme has sparked intrigue because it can, among other dynamical effects, optically induce square-wave (SW) switching with a periodicity slightly longer than 2τ.

High-frequency, regular SWs are interesting for many applications and they have been studied in other optoelectronic systems [20]. Selective orthogonal coupling, such that the dominant mode of one laser is rotated by 90° and then injected into the naturally suppressed mode of another laser (and vice versa for mutual coupling), is also capable of producing optically-induced square-wave switching [21]. With delays that are of a few nanoseconds, a main advantage of the feedback or coupling schemes is that they are capable of producing SWs with a repetition rate in the gigahertz range that is tuned by the delay time of the feedback or of the coupling.

ii. Previous Results

Several experiments have been performed in which only one polarization, the natural lasing one, is selected and fed back into the orthogonal one [22–25].With this scheme, referred to as selective orthogonal feedback, it has been observed that the feedback linearly shifts the laser emission frequency [22,23] and, under strong feedback, polarization SWs have also been observed [24,25]. VCSELs present a polarization behavior that strongly differs from that of EELs; thus, it can be expected that the SWs in these lasers will present different features. For example, [26] demonstrated numerically that in VCSELs with selective orthogonal coupling the square waves are more irregular than those in EELs with selective orthogonal coupling [27,28]. Moreover, while in [27,28] the SWs were found to be stable in narrow parameter regions, in [26] they were just a transient dynamic.

D. Thesis Overview

In this thesis, I study experimentally and numerically SWs in VCSELs induced by selective orthogonal feedback. The primary goal of my work is to find parameters that optimize the regularity of the switchings. This study extends the work of Mulet *et al.* [24] that studied experimentally and numerically a VCSEL with orthogonal feedback. Simulations based on the spin-flip model (covered in section III.B) for VCSELs in [24] and on a two-mode model for EELs in [25] showed a good agreement with the observations. More complex wave forms were also observed, both experimentally and numerically. Also in [24], the laser was pumped close to threshold and the simulations were done with parameters that fitted the experimental situation. For my work, the experiments are done with VCSELs biased well above threshold, and in the simulations, a wide region of parameters is explored. In particular, I study one type of feedback referred to as $x \rightarrow y$ feedback: when the natural mode of polarization x is injected with orthogonal feedback of polarization mode y. I note that in [24], the laser parameters that fitted the experimental situation corresponded to $y \rightarrow x$ feedback. I find that there appears to be an optimal pump current for optimizing square wave stability in our VCSEL, shown through excellent qualitative agreement between our experimental results and numerical simulations for the $x \rightarrow y$ feedback scheme. I further quantify square wave regularity with a statistical study of the mean switching time $\langle T \rangle$. I conclude that the optimal pump current value changes with feedback strength, but also other feedback mechanisms beyond the scope of my current work.

In section II we will explore our experimental investigations through describing our apparatus and data acquisition methods, followed by interpretation and discussion of our experimental findings. Section III will cover the mathematical model that we base our numerical simulations on, and the results we garner from them including square waves, optimum current,

SW degradation and mean switching time. Section IV will provide the framework for possible future work including mutually-coupled VCSELs, and how our current work may lead to it. I conclude my thesis work in section V, summarizing the experiment and future direction of the project.

II. Experimental Investigations

A. Apparatus

In our experiments we employ a VCSEL fabricated to operate in a single longitudinal mode and single transverse mode (Finisar SV3639-001, λ = 856 nm when thermally stabilized at 18.00 °C, having a threshold current I_{th} = 1.18 mA). The stand-alone VCSEL (in the absence of feedback) does not display polarization switching or polarization instabilities.

Our apparatus consists of a laser that receives delayed optical feedback from a distant reflector, with the feedback being rotated in polarization by 90 degrees from the laser's output state. This polarization-rotated feedback can influence the laser in such a way as to periodically switch its polarization state to one that is orthogonal to the original state, a dynamical feature that we exploit to produce square waves. Our experimental apparatus is compartmentalized into two main sections: the feedback loop and the detection area. The process of creating the polarization-rotated feedback occurs in the feedback loop. To observe these square waves, a beam splitter samples off the beam before it enters the feedback loop and sends it to the detection area where we utilize polarization-resolved detection to capture our experimental data.

An experimental note worth explaining before describing the feedback loop in detail involves our utilization of a Faraday rotator (ROT), as opposed to a quarter-wave plate ($\lambda/4$). Both optical devices have the ability to create polarization-rotated optical feedback, meaning we could substitute the quarter-wave plate in and still generate square waves. A $\lambda/4$ plate can take linearly polarized light and produce circularly polarized light via the birefringence of the wave plate material. While circular polarization is not useful for our experiment, if one reflects said light back into the $\lambda/4$ plate it returns to a linear polarization. By aligning the linearly polarized incident beam at 45° relative to the fast axis of the waveplate and retroreflecting the beam back

through, the resulting feedback produced is orthogonal in polarization to that of the incident beam. Previous research has studied the case of using a quarter-wave plate and found that it can produce polarization switching well in EELs (edge-emitting lasers), but with VCSELs the square wave dynamics are not as stable or clean [29]. We simplify our configuration to allow only one particular coupling of linear polarizations (x → y) to learn more about stability. To do this, we elect to use a Faraday rotator for its ability to provide polarization-selective feedback (described in the following paragraph) as opposed to the $\lambda/4$ plate which cannot isolate a particular linear coupling to study.

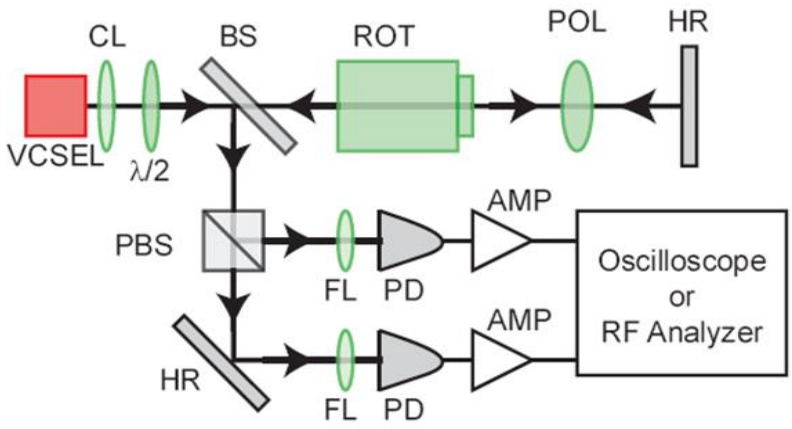

Figure 2.1 Experimental apparatus. The beamsplitter (BS) marks the separation point of the two main regions. The devices along the top level of the diagram make up the feedback loop, while the lower section comprises the detection area.

The experimental setup is shown in Fig. 2.1 above, resting on an isolated vibration-dampening bench. The feedback loop is formed by a linear external cavity of length 153 cm which corresponds to a photon round-trip time of τ = 10.2 ns. For illustrative purposes, I will describe the path our beam travels through this experiment in a qualitative manner.

The laser (VCSEL) emission is first collimated by a lens (CL, Newport F-L20, numerical aperture 0.50). A half-wave plate ($\lambda/2$) compensates for the initially non-Cartesian orientation of the polarization, thus allowing for more accurate 90° feedback rotation and better polarization-resolved detection. This device orients the natural polarization mode of the VCSEL to be

horizontal, which we define as parallel to the table surface. The beam then passes through a nonpolarizing plate beamsplitter (BS) that transmits 70% of the incident power, and continues through a Faraday rotator (ROT), made of a Faraday isolator with the input polarizer removed and output polarizer oriented 45° from horizontal. The beam, now linearly polarized at 45°, passes through a rotatable polarizer (POL) used to control feedback strength, then reflects from a high-reflectivity mirror (HR). On the return path, the beam first passes unchanged through the rotatable polarizer and then reenters the Faraday rotator through its output polarizer. It rotates yet another 45° travelling through the Faraday isolator resulting in a total rotation of 90°, and finally passes through the $\lambda/2$ plate so it is reinjected into the VCSEL in a polarization state orthogonal to the natural mode of emission. I will refer to this feedback as vertically polarized or simply vertical.

If the vertical feedback is strong enough, it can suppress the laser's dominant polarization mode (horizontal) and produce vertical emission. Following the path of the vertical emission, it enters the Faraday rotator and rotates 45° as expected. However, by the time it reaches the output polarizer, the polarization has been oriented perpendicular to the transmission axis and the beam is extinguished. This selectivity assures the feedback arises from only a single round trip in the external cavity, meaning that the external cavity length governs the time between switches in polarization states of the laser. After roughly 10.2 ns, the polarization state reverts back to its solitary (horizontal) state, since vertical emission in this case can last only as long as it is supplied vertical feedback. This switching effect is the primary goal of our configuration: it creates polarization-selective feedback such that horizontal emissions can produce vertical feedback ($x \rightarrow y$), but vertical emissions are extinguished by the output polarizer of the Faraday rotator.

B. Data Acquisition

For our experiment, polarization-resolved detection is needed to observe the dynamical effects most clearly. We remind ourselves that the beam we are detecting is sampled prior the feedback loop so that we may detect both polarization states. The reflected beam (30% incident beam strength) from the plate beamsplitter (BS) is steered to a polarizing beamsplitter cube (PBS). The two resulting beams travel along separate detection paths each consisting of a focusing lens (FL) which concentrates its beam onto an ac-coupled photodetector (PD, Hamamatsu C4258-01, 8.75 GHz bandwidth). A wideband amplifier (AMP, 10 kHz to 12 GHz, 23-dB gain) strengthens each PD signal. The low end of its frequency range detects our square wave pulses which operate on the MHz range, while the high range provides us with the ability to detect higher possible frequency behavior but also get finer detail on our low frequency readings. The amplified signal is then captured and analyzed with a digital storage oscilloscope (LeCroy 8600, 6-GHz analog bandwidth) or microwave spectrum analyzer (Agilent E4405B). These two devices allow us to either analyze data in the time or frequency domains for both polarization states simultaneously; however, we primarily focus on gathering time sequence data. For the data displayed in Fig. 2.2, we used a sample rate of 20 kS/s over 1 μs, yielding 20,000 data points with a 50 ps time interval between each point.

C. Experimental Challenges

While I have described the process of achieving square waves to be as simple as taking a laser and shining it back at itself with rotated feedback, physically constructing and fine-tuning the apparatus was quite a challenge. For the feedback loop, we overcame two major obstacles:

aligning the free-space optical devices with the beam path, and creating a near-perfect collinear beam in the external cavity. The device issues were primarily with the Faraday rotator: not only did we have to align the beam with the input aperture, but also the aperture of the output polarizer. In other words, we must thread a tube with the laser beam, not just hit a point. This precision alignment could take an experienced lab assistant several hours to complete, especially considering the moderate degree of mechanical relaxations present in the adjustable base mounts.

Upon completing the device alignment in the feedback loop, the next objective was to bounce the reflected beam right back on the incident beam. This step is necessary for our experiment, as it ensures the polarization-rotated feedback is aimed directly at the laser. This process was made difficult by working with a laser beam whose wavelength is beyond the visible spectrum of light. To make the infrared beam collinear with itself, we developed an alignment tool that consisted of two infrared detecting cards taped together (detection sides facing out) with a small hole punched through both of them. Once the incoming beam passed through the hole, you could detect the reflected beam's path on the backside of the first. By using sensitive mirror adjustment techniques, we could align the reflected beam so that it past right back through the opening in the card it came through, thus achieving a collinear beam. To fine tune the mirror alignments, we placed a power meter in the detection path for vertically-polarized light and adjust the mirrors until we reach a power maximum. This process provides a solid indicator of the amount of vertical feedback the laser is receiving as noted in the strength of its vertical emission.

D. Experimental Findings

i. VCSEL Square Waves

Experimental results demonstrate that self-modulated square waves produced by the VCSEL in this configuration tend to be noisy and disordered, but can be optimized by the pump current for a given feedback strength. Figure 2.2 displays time series that illustrate the current dependence of the square waves.

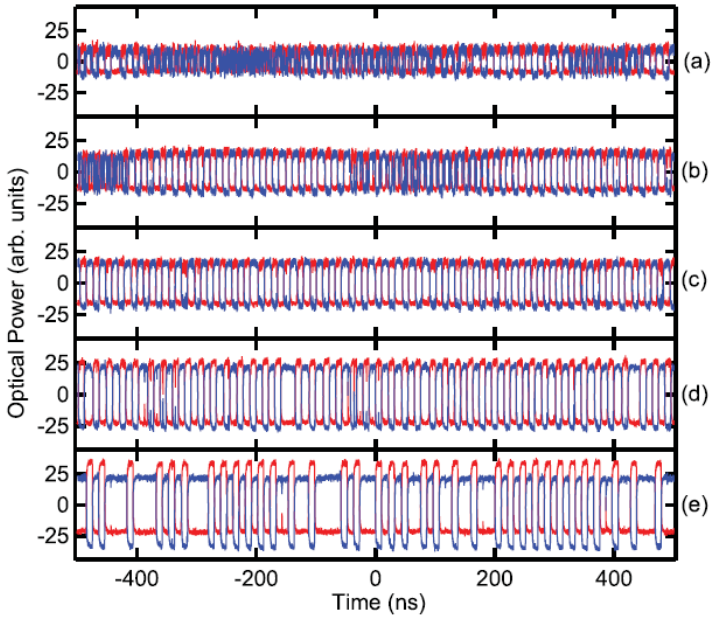

Figure 2.2 Experimental time series of the intensity of both polarization modes of a VCSEL with PR feedback at various pump currents for fixed feedback strength. Pump currents are (a) 2.20 mA, (b) 2.60 mA, (c) 2.75 mA, (d) 3.20 mA, and (e) 3.40 mA. The horizontal polarization (the natural lasing mode) is shown in red, and the vertical polarization (the suppressed mode) in blue.

For all time-series shown in Fig. 2.2, the delay time is τ = 10.2 ns and the round-trip power transmission is 30.6%. Each graph shows both polarization modes, captured simultaneously and deskewed to compensate for the 0.45-ns difference in detection path length. The horizontal polarization, which is the natural lasing mode, is shown in red and the vertical polarization (the suppressed mode) in blue.

The switching regularity, a primary indicator of square wave stability, appears to be optimal at I = 2.75 mA (Fig. 2.2(c)) for this experiment. We do not find perfect square waves, which could be explained by a few different reasons. One such cause could be that the internal

noise affects laser dynamics, leading to complex behavior ultimately impacting the periodicity of our SWs. In other words, our optimum current describes where these instabilities are minimized, not completely absent. We reaffirm this particular value much like one focuses a blurry image: we check the stability at pump currents above and below our optimum value, finally settling at the ideal current. Below this current value, the waves degrade by exhibiting rapid oscillations that disrupt the square-wave plateaus. Above the optimum value, the regularity is also degraded, with longer intervals appearing irregularly between square pulses for the vertically polarized light. Again, the timing of the switchings is not perfectly regular at our optimum current, but the irregularities are minimized. Other time traces at this setting (not shown) indicate that there are occasional interruptions similar to those in Fig. 2.2(b), but they occur less often.

Further experiments carried out at other feedback strengths suggest that an optimal current exists for switching regularity, but can vary with feedback strength (shown in section II.E). However, we also find that the cleanest and most regular square waves occur when feedback is strong.

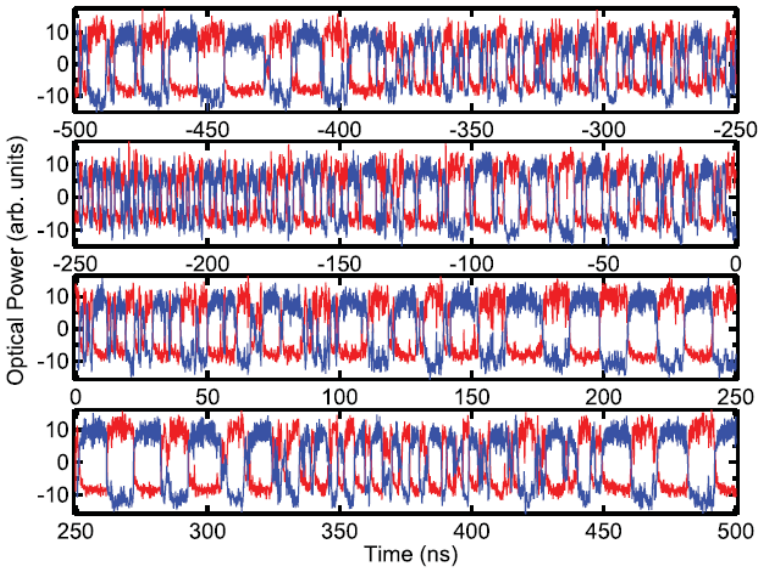

Figure 2.3 Experimental time series of the intensity of both polarization modes of a VCSEL with PR feedback. External cavity transmission ratio is 30.6% and pump current I = 2.20 mA. All four graphs are close-up views at the data displayed in Fig. 2.2(a).

Figure 2.3 examines in greater detail the 1-μs time series shown in Fig. 2.2(a), with pump current I = 2.20 mA. Different levels of complex behavior are seen, such as almost regular switching, regions where the plateaus become disordered with spikes or holes, and regions of rapid oscillation where the 4L/c periodicity is not apparent. The transitions between these shapes do not appear to be abrupt, and therefore are likely to be a manifestation of noise-driven instability rather than a bifurcation to different solutions. To further demonstrate that the above observations are generic, in section III we simulate the VCSEL behavior using the spin-flip model as a framework. We employ parameter values that are typically used for modeling VCSEL dynamics, and only the feedback delay time is chosen to fit the experimental value.

E. Statistical Analysis

i. Overview

To complement the qualitative nature of our experimental results presentation, I now turn to a more quantitative approach: mapping out a particular region of parameter space (μ, η). By taking time-sequence data at a range of pump currents and feedback strengths, various sorting programs and analysis tools allow us to extract relevant statistical measures from each set. By looking at the mean switching time $\langle T \rangle$ (which should ideally be 2τ) and its standard deviation σ_T, we can better determine which set of parameter values best represent the optimal conditions for SW regularity. This type of analysis can also shed light on how SW stability is affected when one parameter is held constant while the other varies. For this section, I keep the same experimental apparatus utilized in Section II.D. Our study was performed using a different laser than in our initial experiment, but still of the same model (Finisar SV3639-001). This laser

demonstrates different characteristics than our previous laser, primarily a lower optimal current range for stability. In this subsection I explain the process of selecting and capturing time-sequence data across a set of parameters, smoothing the raw data to filter out excess noise and anomalies, and my utilization of a sorting program to extract relevant statistical data from the smoothed time-sequence data.

ii. Methodology

The parameter space I explore includes pump currents ranging from $\mu = 2.0$ mA to $\mu = 2.4$ mA (incremented by 0.1 mA) and 8 different values of feedback strength η. Referring back to our experimental apparatus (Fig. 2.1), I manipulate η by means of rotating the polarizer (POL) and choose to sample at equally-spaced angle increments of 5° starting from slightly off full feedback strength. To present these angles in this study would not provide information about the amount of power being sent back to the laser; thus, I express η as the roundtrip transmission ratio (RTR) expressed as a percent of the total output power of the solitary VCSEL for each respective μ value I sample.

I record 40 sets of time-sequence data stemming from my selection of 5 pump currents and 8 feedback strengths, using the same digital oscilloscope from our previous experiment (LeCroy 8600, 6-GHz analog bandwidth). Data from only one polarization state is captured, as it contains all the information we need for our study (explained in next paragraph). The statistical aspect of this undertaking necessitates a longer time interval to sample than our previous 1 μs interval (yielding 20,000 data points) from section II.B. We adjust the oscilloscope to record data for 20 μs, resulting in 400,000 data points per set (sample rate kept at 20 KS/s).

To produce statistical figures from the sheer volume of data gathered (40 sets of 400,000 data points adds to 16 million power/time pairs), I develop a sorting program (Appendix A) to extract periodicity information from a given set of time-sequence data to be used in calculating $\langle T \rangle$ and σ_T. The program first pulls out every zero-crossing in the time-sequence data, indicative of a switch in polarization state or noisy signal. From that list of points where sign change occurs, a subroutine then takes the difference between the first and last point of a set of 3 time points (generalized to points t, $t-1$ and $t-2$). This difference in time measures the switching time (periodicity) of that particular segment. The program preforms this subroutine across all the zero-crossing points and generates a list of all the periods within a given time-sequence set. This list of periods allows us to calculate $\langle T \rangle$ and σ_T for each parameter set (μ, η).

Having laid out the main discourse on our methods of analysis, I choose to introduce an intermediary step between data collection and sorting for periodicity. The raw data, even sets found to have optimal SW regularity for the laser, contain extraneous noise; if not filtered out, the rapid zero-crossing that result would skew our data, given the methodology presented. To reduce the effects of this noise, I first import the raw time-sequence data into Data Studio, an application capable of creating time-averaged curve fits from noisy signals. I utilize Data Studio's smoothing function and adjust its effect by visual inspection to account for signal degradation where it should and also rule out trivial noise near the axis crossing. Overall, this extra stage in processing is designed to enhance the effectiveness of my sorting program while still accurately representing the actual data collected.

iii. Mean Switching Time

At the bottom of this page and the top of the next, I present the statistical data gathered from my parameter space study (Fig. 2.4, 2.5). One indicator of square wave stability is studying the mean switching time $\langle T \rangle$ across parameter space. We take the switching time to be how long the laser takes to cycle between the two polarization states (in other words, the length of two plateaus). The fewer irregular oscillations we see in a set of time series data, the closer we expect the average switching time to be to 2τ. Based on this criteria, I find that the most stable square-waves occur at lower η (roughly $12 - 19$ % RTR) with μ affecting these regions only slightly. Another useful figure we utilize involves looking at the standard deviation σ_T of the mean switching time, which tells us about the spread of T values in a given data set. Conceptualizing this idea, if we had a set of perfect squares waves in a time-sequence with each plateau having a length of τ, we would expect to find that $\sigma_T = 0$. We will call upon these statistical measures

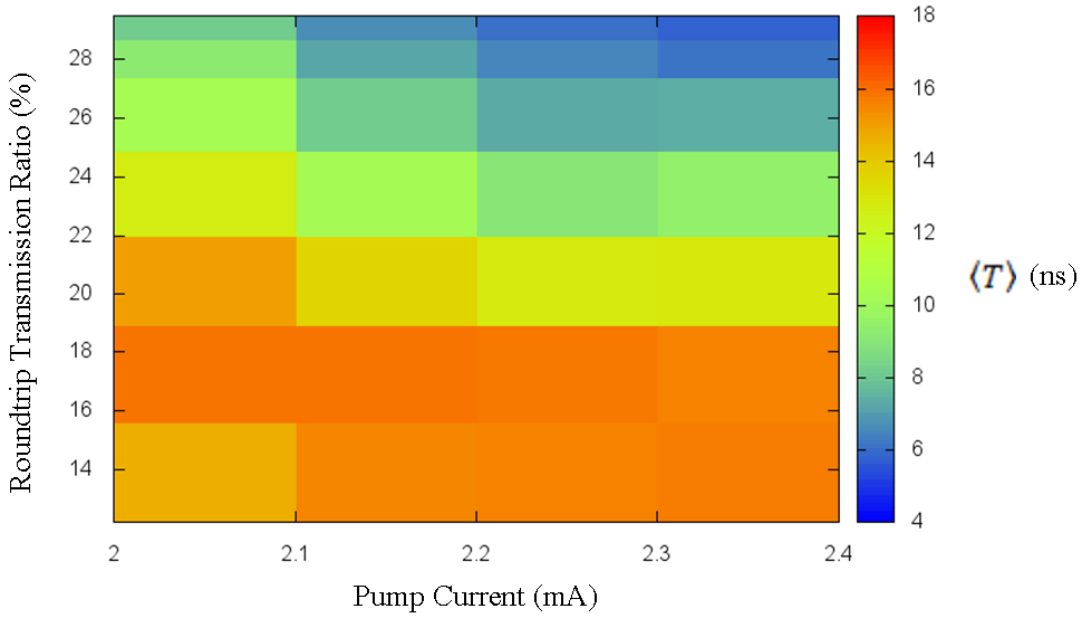

Figure 2.4 Contour plot for mean switching time $\langle T \rangle$ across (μ, η) parameter space (above). Values of $\langle T \rangle$ were extracted by means of the methodology outlined in the main text (section II.E.ii). Note the axes tick marks match up to points, not blocks of color—the colors are influenced by the other $\langle T \rangle$ values surrounding each point. Compared to our results from section II.D, we would expect $\langle T \rangle$ to be closer to 2τ in at higher η. However, we will see later with our numerical studies that this region of parameter space is quite small and open to many interpretations.

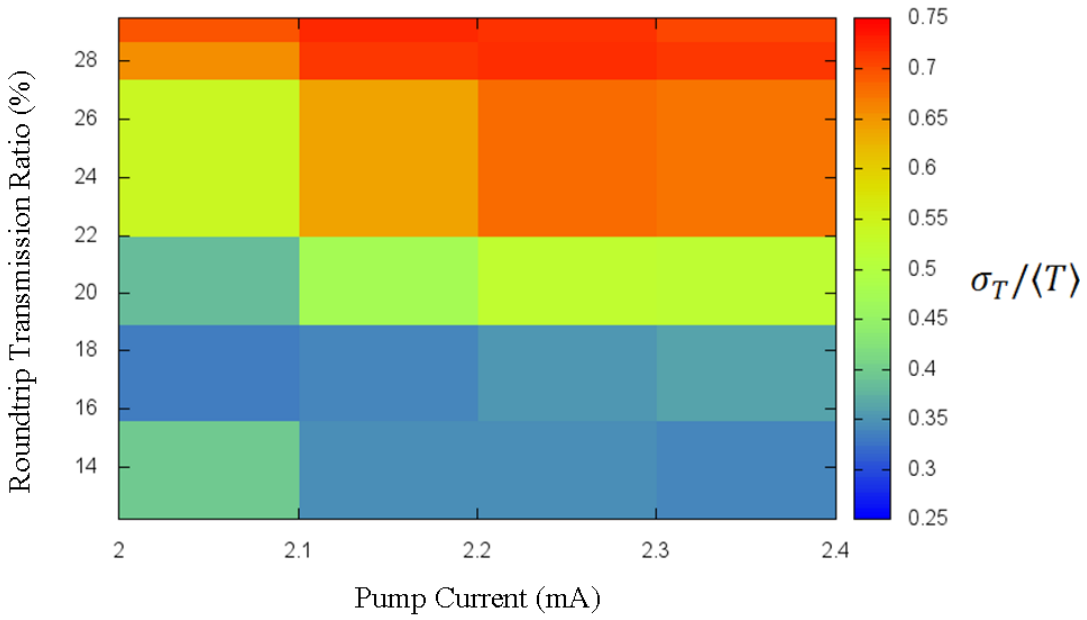

Figure 2.5 Contour plot for the ratio $\sigma_T/\langle T\rangle$. We present the σ_T values this way to better represent their relationship to their respective $\langle T\rangle$. In combination with Fig. 2.6, a better conceptual picture of square wave stability materializes with information on not only the mean switching time but also how much it fluctuates away from that average.

later in section III.C.

This particular laser and parameter space do not display the correlation of higher η with more stable square waves that we found in our earlier experimental study (section II.D), which can be interpreted several ways. From both Figs. 2.4 and 2.5, we see a relatively small region of parameter space that displays a wide range of dynamical behavior from highly unstable oscillations to square wave with near optimal switching regularity. Figure 2.4 does highlight one element of our previous conclusion, seen on the far left side: looking at the color pattern, we see that there is an optimal feedback strength for $\mu = 2.0$ mA when η corresponds to an RTR of around $16 - 18\%$. Numerical results shown later in section III.C provide comparison for better understanding square wave stability, albeit in a different but wider parameter space.

III. Mathematical Model

A. Lang-Kobayashi Model

After the birth of EELs in the early 1960's, a mathematical model was developed to model the behavior of semiconductor lasers [1]. The semiconductor laser rate equations (SLREs) consists of two rate equations, one which governs the complex electric field amplitude *E* of the laser beam and another modeling the rate of change in carrier number *N* within the gain medium.

$$\frac{dE}{dt} = (1 + i\alpha)NE \tag{3.1}$$

$$T\frac{dN}{dt} = P - N - (1 + 2N)|E|^2 \tag{3.2}$$

Equations (3.1) and (3.2) represent the dimensionless (meaning they can be expressed with any choice of parameters) SLREs for a solitary singlemode EEL with linewidth enhancement α, pump parameter above threshold *P*, and ratio of carrier to photon lifetimes given by *T*. Equation (3.1) has roots in first principles, originating from Maxwell's equations in a dielectric medium in conjunction with a wave equation involving a polarization source term. However, the model as a whole is a phenomenological one, with Eq. (3.2) being designed to agree with physical observations of the gain medium instead of stemming from first principles. We treat the SLREs as a semiclassical model, describing the electric field equation using classical (Maxwellian) physics and addressing the gain medium with quantum mechanics. Looking at the two equations symbolically, their interconnectedness is visible on a surface level: *E* plays a part in (3.2) as a squared amplitude term, and *N* acts as a multiplicative factor in (3.1), contributing (or restricting) the change in *E*. Together, these equations can provide both steady state and dynamical solutions describing EEL behavior.

The Lang and Kobayashi (LK) equations [30] came in 1980, brought on by an increase in study of optical feedback and its dynamical effects on semiconductors lasers. The LK equations took the SLREs and incorporated a delay term in the electric field equation to account for the effects of conventional (non-rotated) optical feedback.

$$\frac{dE}{dt} = (1 + i\alpha)NE + \eta E(t - \tau) \tag{3.3}$$

$$T\frac{dN}{dt} = P - N - (1 + 2N)|E|^2 \tag{3.4}$$

Equation (3.3) keeps the same form as Eq. (3.1), but gains the added delayed feedback term. This second term denotes the injection strength η combined with electric field information received at delayed rate τ, corresponding to the external cavity length of the configuration. In the next subsection, we will show how the Lang-Kobayashi approach serves as a stepping stone for our experimental setup.

B. Spin-Flip Model

Previously in section II, we discussed that EELs and VCSELs differ in their structure and resulting energy bands: as a result, where EELs can be modeled using only one carrier rate equation, VCSELs require two. VCSELs have two allowed transitions between the conduction and valence band: for total angular momentum $J_z = -1/2$ to $J_z = -3/2$, and from $J_z = 1/2$ to $J_z = 3/2$, which model two entirely different carrier populations [31]. Thus, the original SLREs cannot fully model this new system; we instead use the spin-flip model (SFM) [32]. The SFM provides for VCSELs what the SLRE model did for EELs: a set of rate equations that provide numerical and analytical solutions for VCSEL dynamics. We apply the work of LK to this

model, incorporating time-delayed feedback terms into the complex electric field amplitude rate equations. We utilize a set of four rate equations (3.5 – 3.8) to model our experimental configuration. Note the similarities between the SFM and SLRE: while the SFM has two more equations, both seek to model laser dynamics using rate equations for electric fields and carrier numbers.

$$\frac{dE_x}{dt} = k(1 + i\alpha)\big[(N-1)E_x + inE_y\big] - \big(\gamma_a + i\gamma_p\big)E_x + \xi_x\sqrt{\beta_{sp}} \tag{3.5}$$

$$\frac{dE_y}{dt} = k(1 + i\alpha)\big[(N-1)E_y - inE_x\big] + \big(\gamma_a + i\gamma_p\big)E_y + \xi_y\sqrt{\beta_{sp}} + \eta E_x(t-\tau) \tag{3.6}$$

$$\frac{dN}{dt} = \gamma_n[\mu - N - NI - in(E_yE_x^* - E_xE_y^*)] \tag{3.7}$$

$$\frac{dn}{dt} = \gamma_s n - \gamma_n[nI - iN(E_yE_x^* - E_xE_y^*)] \tag{3.8}$$

Here, E_x and E_y are orthogonal linearly polarized field amplitudes, N and n are two carrier densities, $I = |E_x|^2 + |E_y|^2$, k is the field decay rate, γ_n is the carrier decay rate, and γ_s is the spin-flip rate. We denote the linewidth enhancement factor as α, and γ_a and γ_p are the dichroism and birefringence parameters: for $\gamma_a > 0$ ($\gamma_p > 0$) the y polarization has a lower threshold (a higher frequency) than the x polarization. The injection current parameter is given by μ, β_{sp} is the strength of spontaneous emission noise, and $\xi_{x,y}$ are uncorrelated Gaussian white noises. We include these white noise terms in our model to account for the inherent noise generated by the laser itself. The feedback parameters are the injection strength η and the delay time τ. The orthogonal feedback term in Eq. (3.6) is $\eta E_x(t-\tau)$, which explicitly denotes the relationship of horizontal feedback strength influencing the vertically-polarized electric field rate equation.

C. Numerical Results

i. Square Waves

We conduct numerical simulations based on the SFM to study the dynamics of the VCSEL and to confirm, validate and interpret our experimental results. The first thing we must do to perform numerical simulations is assign values to the constants used in (3.5 – 3.8). Unless otherwise specifically stated, we set the parameters to be $k = 300\ \text{ns}^{-1}$, $\gamma_n = 2\ \text{ns}^{-1}$, $\gamma_s = 50\ \text{ns}^{-1}$, $\gamma_a = 0.4\ \text{ns}^{-1}$, $\alpha = 3$, $\beta_{sp} = 10^{-4}\ \text{ns}^{-1}$, $\eta = 50\ \text{ns}^{-1}$, and $\tau = 10$ ns. The pump current μ and the birefringence γ_p are taken as control parameters. Because the experiments were done well above threshold, we will mainly consider values of $\mu \geq 2$.

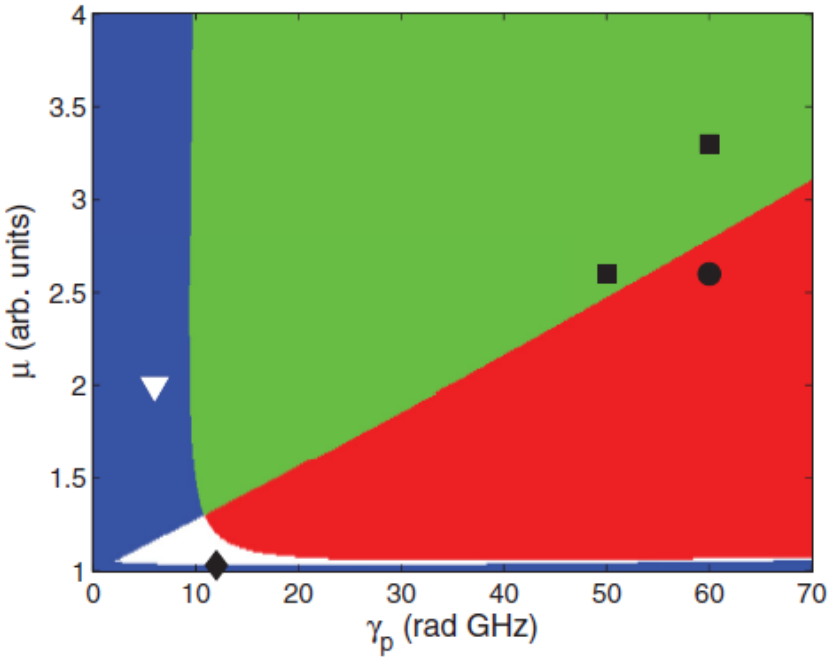

Figure 3.1 Stability diagram of the *x* and *y* polarizations of the solitary VCSEL in the parameter space (birefringence, pump current). Red and blue indicate regions of polarization monostability (red, lower right region: only the *x* polarization is stable, blue region on the left: only the *y* polarization is stable); white indicates the region of polarization bistability (both polarizations are stable); green indicates the region where CW output in *x* or *y* polarization is unstable. The model parameters are as indicated in the text, and the symbols indicate the values of μ and γ_p used in Fig. 3.2 and other experiments that were omitted from this paper.

The parameter γ_p will be chosen such that the solitary laser is monomode and emits either the *x* or the *y* polarization. In Fig. 3.1, which displays the linear stability of the *x* and *y* polarizations,

one can observe that well above threshold the x polarization is stable for large γ_p, while the y polarization is stable for low γ_p. Therefore, to analyze the dynamics with $x \rightarrow y$ feedback, we will choose γ_p large; if we wanted to analyze the dynamics with $y \rightarrow x$ feedback, we would choose γ_p small. For parameters where the x polarization is stable for the solitary laser, with moderate $x \rightarrow y$ feedback strength, regular square-wave switching is observed, as shown in Fig 3.2(a). The dynamics with $x \rightarrow y$ feedback is displayed in Figs. 3.2(b) and 3.2(c), where one can observe that the y polarization lases all the time, switching between two intensity plateaus, one higher than

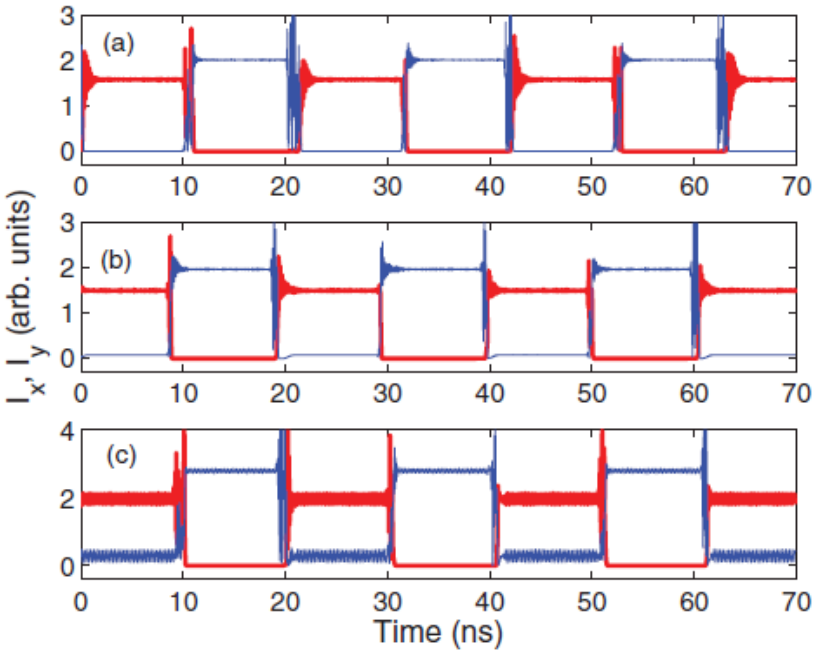

Figure 3.2 Intensities of the x (red) and y (blue) polarizations with $x \rightarrow y$ feedback. The parameters are γ_p = 60 rad GHz and μ = 2.6 (a), γ_p = 50 rad GHz and μ = 2.6 (b), γ_p = 60 rad GHz and μ = 3.3 (c); other parameters are as indicated in the text.

the solitary laser intensity and one slightly above the noise level. Other simulations for y → x feedback were performed and exhibit different features than shown here; however, our focus here is on the direct comparison of numerics to our experimental results.

ii. Optimal Current

For certain parameters a variation of the injection current can affect the regularity of the switchings; this is displayed in Fig. 3.3 for $x \rightarrow y$ feedback. In this figure the intensities were

filtered to simulate the 6-GHz experimental bandwidth of our oscilloscope. There is an optimal range of pump current values where the switching is very regular; for lower μ, intervals of regular switchings alternate with intervals of irregular oscillations, while for higher μ, the switchings degrade to irregular oscillations. One can notice a qualitatively good agreement with the experimental observations (Fig. 2.2), but we also note differences between experiment and theory. In the experiments the amplitude of the square-wave switching appears to be the same for both modes (Fig. 2.2), while in the simulations they are slightly different (see Fig. 3.2).

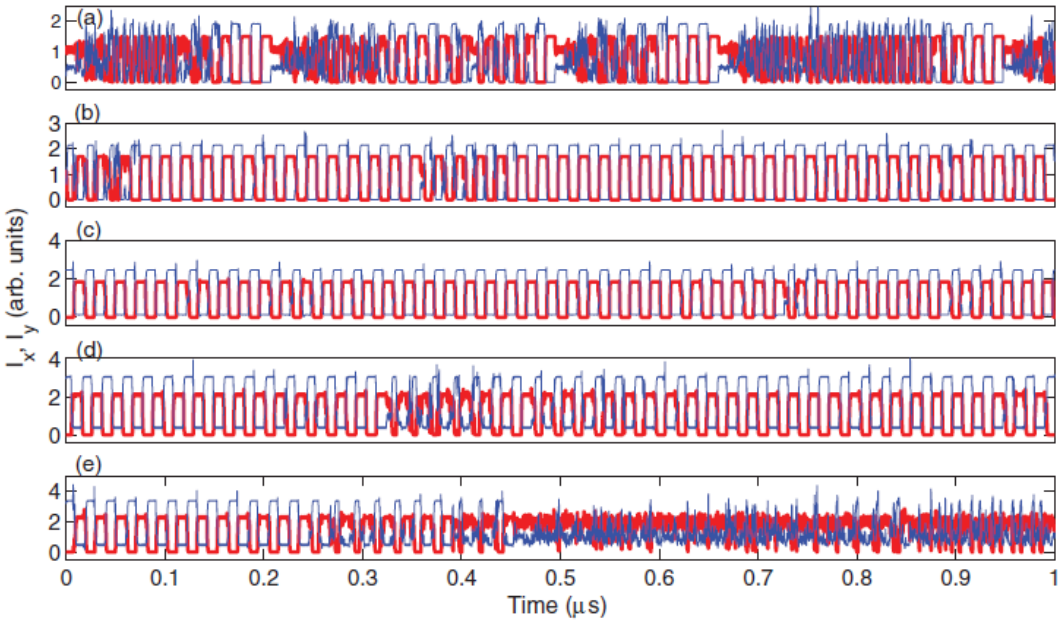

Figure 3.3 Numerical simulations for $x \rightarrow y$ injection (red line: x polarization, blue line: y polarization). I_x and I_y were filtered to simulate the 6-GHz experimental bandwidth. μ = 2.5 (a), 2.7 (b), 3.0 (c), 3.5 (d), and 3.8 (d), η = 50 ns^{-1}, γ_p = 60 rad/ns; other parameters are as indicated in the text.

Also, we were unable to simulate the wider plateaus experimentally found at higher pump currents (Fig. 2.2(d), 2.2(e)). To further investigate these questions, a more thorough matching of numerical constants to our laser's specifications would be beneficial.

iii. Mean Switching Time

In following our experimental goal to find more stable square waves, we need to analyze the time series data our numerical simulations present us with. This provides a follow up to statistical analysis performed on our experimental results in section II.E, which involved a relatively space region of parameter space. Since numerical simulations can quickly predict a wide range of behavior, a much greater region of parameter space is explored. This includes spotting interesting trends that can lead to better overall understanding of the different mechanisms that contribute to square-wave stability and regularity.

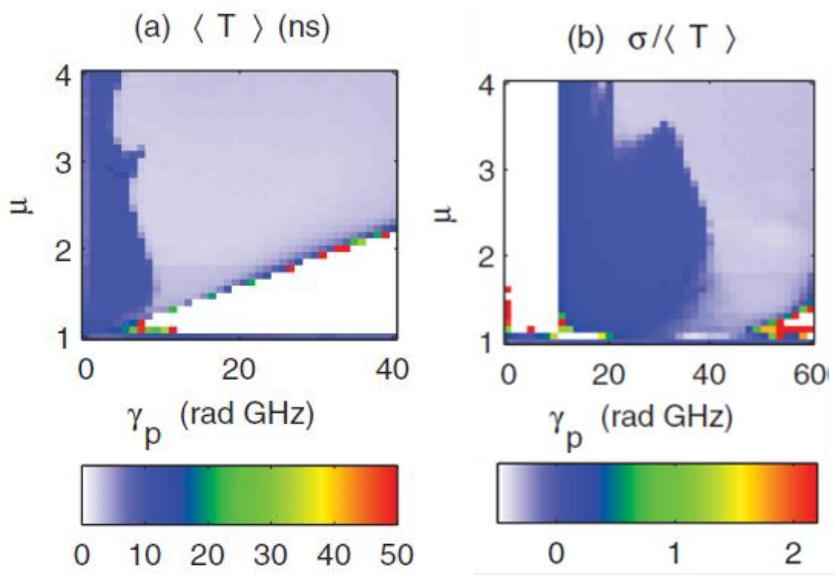

Figure 3.4 Mean switching time (a), and its normalized standard deviation (b). Both plot the birefringence vs. pump current parameters for $x \rightarrow y$ feedback. The vertical lines in panel (b) indicate variations of μ that affect the switching regularity as observed in the numerical simulations. η = 30 ns^{-1}; other parameters as indicated in the text. In the white regions no polarization switchings occur; in the red regions, $\langle T \rangle$ > 50 ns.

Using the two methods of analysis described in section II.E.iii, we quantify the degree of switching regularity as shown in Fig. 3.4 where we plot the average switching time $\langle T \rangle$ and its normalized dispersion $/\langle T \rangle$, both plotted against our parameters μ and γ_p. In this figure one can observe that there are parameter regions where increasing μ results in first a decrease, followed by an increase of the switching regularity $\sigma/\langle T \rangle$ reaching a minimum at specific current values that depend on the value of γ_p, as observed in the experiments. For parameters near the borders of

the monostability regions of the solitary laser, the mean switching time becomes increasingly long until the switchings eventually disappear [the red color in Figs. 3.4(a) indicates $\langle T \rangle > 50$ ns]. In Ref. [24] the degradation of the switching was understood as the result of a change of stability of the solitary laser polarizations. However, for parameters considered here (which are well above threshold) the degradation of the square waves is not related to a change of stability of the solitary laser modes.

IV. Future Direction

As scientists continue to expand the fundamental understanding of VCSEL dynamics when they are subjected to orthogonal feedback, there will always be more work to be done. Further research can be carried out regarding how specific experimental elements and inherent laser properties contribute to SW degradation and switching regularity, extending the boundaries of parameter space beyond the scope of the work presented in this thesis.

Upon having satisfactorily studied a single VCSEL in our rotated feedback regime, another experiment to investigate would be SW optimization in an experimental apparatus containing mutually-coupled VCSELs (Fig. 4.1).

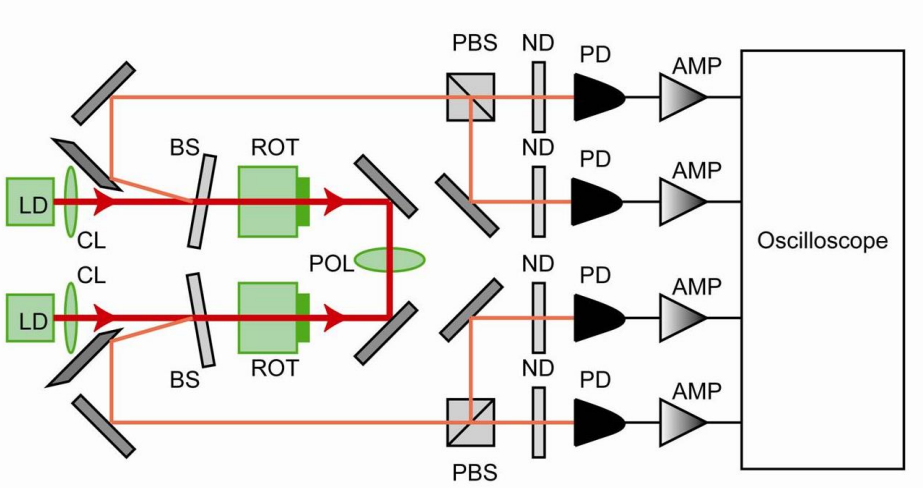

Figure 4.1 Schematic diagram for mutually-coupled VCSEL experiment; note the symmetry and similar structure when compared with Fig. 2.1. Feedback arises from each VCSEL being rotated and injected orthogonally into the other; each beam passes through both Faraday rotators (ROT) once, simulating the beam retroreflection (thus 90° rotation) we use in our experiment. Both beams are sampled off for polarization-resolved detection prior to entering the feedback regime.

As with much research in semiconductor laser dynamics, this experiment involving EELs has been studied [PRA 20] but remains to be investigated with VCSELs. Such an apparatus as Fig. 4.1 introduces a variety of new dynamics beyond our single-VCSEL experiment, but could further expand our understanding of VCSEL dynamics and their applications in technology.

V. Summary and Conclusion

In this thesis, we studied the experimental and numerical dynamics of VCSELs with selective orthogonal feedback and found that the switching dynamics are noisier than in EELs, but also that parameters can be found to optimize switching regularity. Such parameters included feedback strength η and pump current μ, both easily manipulated in our experimental apparatus. The numerical simulations of time-sequence data for the $x \rightarrow y$ feedback regime are in qualitatively good agreement with our experimental observations. The numerics also indicate that for the $x \rightarrow y$ feedback case, there is a wider parameter region where regular switching can be observed (as compared to $y \rightarrow x$ in [24].

The simulations also suggest that at high μ ($\mu > \mu_{th}$), the switching dynamics are less affected by the inherent noise, as compared to μ values close to threshold [24]. In addition, at high μ the degradation of the regularity of the switchings is not accompanied by a change of the stability of the solitary laser modes (as it occurs at lower pump current [24]), and thus, it will be interesting to investigate in a future work which mechanisms are involved in the degradation of the switching regularity.

VI. Appendix A

Below is the C++ program code used in section II.D.ii for the statistical study of switching regularity. The program is designed to take an input .txt file containing smoothed time-sequence data and convert it two separate arrays for power and time, respectively. Once that is accomplished, the arrays are sorted to pull out the corresponding time points whenever the amplitude changes signs (positive to negative or vice versa) and exports them as a .txt file. From those points, a second routine pulls out period information by looking at the time difference between points t and $t-2$.

```
#include <fstream>
#include <iostream>
#include <vector>
using namespace std;

int main ()
{
  ifstream file;
  ofstream output;
  float* time;                                  //Setting up arrays to take input from raw data
  time = new float[400000];
  float* power;
  power = new float[400000];
  vector<float> period(0);

  file.open("input.txt");                       //Change to whatever smoothed data file is called
  file.precision(8);

  for (int i=0; i < 400000 ; i++)               //for-loop governing the transfer of the input data to power and time arrays
  {
    file >> time[i] >> power[i];
  }
  file.close();                                 //Closing input file

  output.open("TimeOutput.txt");                //Opening output file
  output.precision(8);

  for (int j=1; j < 400000; j++)                //for-loop sorting out the zeros into output .txt file
  {
    float result = power[j] * power[j-1];
    if (result < 0)
    {
      output << time[j] << endl;
      period.push_back(time[j]);
    }
  }
  output.close();
  output.open("PeriodOutput.txt");

  for (int t=2; t < period.size(); t+=2)        //for-loop defining periods
  {
   output << period[t] - period[t-2] << endl;
  }
  output.close();

  cout << "Program complete!" << endl;
  system( "PAUSE" );
  delete power;
  delete time;

  return(0);
}
```

VII. Bibliography

[1] Tartwijk, G. v. *Semiconductor Laser Dynamics with Optical Injection and Feedback.* Doctoral dissertation. Vrije Universiteit Amsterdam. 1994.

[2] Einstein, A. On the quantum theory of radiation. Z. Phys., 18:121. 1917.

[3] Hecht, E. *Optics,* 4th ed. pp. 590. USA: Pearson Addison Wesley, 2002.

[4] Lapin, Z. J. Polarization dynamics in a multi-transverse-mode vertical-cavity surface-emitting laser (VCSEL) subject to optical feedback. Honors thesis. Bates College. 2008, and references therein.

[5] Erneux, T., and P. Glorieux. *Laser Dynamics*. Cambridge, UK: Cambridge University Press, 2010.

[6] Erneux, T. *Applied Delay Differential Equations.* New York: Springer Science + Business Media, 2009.

[7] Kane, D., and A. Shore, eds. *Unlocking Dynamical Diversity: Optical Feedback Effects on Semiconductor Lasers*. New York: Wiley and Sons, 2005.

[8] Ohtsubo, J. *Semiconductor Lasers: Stability, Instability, and Chaos*, 2nd ed. Berlin: Springer, 2007.

[9] Lüdge, K., ed. *Nonlinear Laser Dynamics: From Quantum Dots to Cryptography*. Reviews in Nonlinear Dynamics and Complexity. Wiley-VCH Verlag GmbH & Co. KGaA, 2012.

[10] Loh, W. H., Y. Ozeki, and C. L. Tang. High-frequency polarization self-modulation and chaotic phenomena in external cavity semiconductor lasers. *Appl. Phys. Lett.* 56:2613-2616, 1990.

[11] Jiang, S., Z. Pan, M. Dagenais, R. A. Morgan, and K. Kojima. High-frequency polarization self-modulation in vertical-cavity surface-emitting lasers. *Appl. Phys. Lett.* 63:3545-3547, 1993.

[12] Robert, F., P. Besnard, M. L. Charles, and G. Stephan. Polarization modulation dynamics of vertical-cavity surface-emitting lasers with an extended cavity. *IEEE J. of Quantum Electron.* 33:2231-2239, 1997.

[13] Sciamanna, M., F. Rogister, O. Deparis, P. Megret, M. Blondel, and T. Erneux. Bifurcation to polarization self-modulation in vertical-cavity surface-emitting lasers. *Opt. Lett.* 27:261-263, 2002.

[14] Heil, T., A. Uchida, P. Davis, and T. Aida. TE-TM dynamics in a semiconductor laser subject to polarization-rotated optical feedback. *Phys. Rev. A* 68:033811, 2003.

[15] Cheng, D.-L., T.-C. Yen, J.-W. Chang, and J.-K. Tsai. Generation of high-speed single-wavelength optical pulses in semiconductor lasers with orthogonal-polarization optical feedback. *Opt. Commun.* 222:363-369, 2003.

[16] Gavrielides, A., T. Erneux, D. W. Sukow, G. Burner, T. McLachlan, J. Miller, and J. Amonette. Square-wave self-modulation in diode lasers with polarization-rotated optical feedback. *Opt. Lett.* 31:2006-2008, 2006.

[17] Takeuchi, Y., R. Shogenji, and J. Ohtsubo. Chaotic dynamics in semiconductor lasers subjected to polarization-rotated optical feedback. *Appl. Phys. Lett.* 93:181105, 2008.

[18] Takeuchi, Y., R. Shogenji, and J. Ohtsubo. Chaos dynamics in semiconductor lasers subjected to polarization-rotated optical feedback. *Optical Review* 17:144-151, 2010.

[19] Xiang, S., W. Pan, L. Yan, B. Luo, X. Zou, N. Jiang, and K. Wen. Influence of polarization mode competition on chaotic unpredictability of vertical-cavity surface-emitting lasers with polarization-rotated optical feedback. *Opt. Lett.* 36:310-312, 2011.

[20] Peil, M., M. Jacquot, Y. K. Chembo, L. Larger, and T. Erneux. Routes to chaos and multiple time scale dynamics in broadband bandpass nonlinear delay electro-optic oscillators. *Phys. Rev. E* 79:026208, 2009.

[21] Sukow, D. W., A. Gavrielides, T. Erneux, B. Mooneyham, K. Lee, J. McKay, and J. Davis. Asymmetric square waves in mutually coupled semiconductor lasers with orthogonal optical injection. *Phys. Rev. E* 81:025206(R), 2010.

[22] Masoller, C., T. Sorrentino, M. Chevrollier, M. Oria. Bistability in Semiconductor Lasers with Polarization-Rotated Frequency-Dependent Optical Feedback. *IEEE J. of Quantum Electron.* 43:261-268, 2007.

[23] Sorrentino, T., O. Di Lorenzo, L. C. de Oliveira, M. Chevrollier, and M. Oria. All-optical frequency-controlled frequency switch. *J. of Opt. Soc. Am. B* 27:1458-1463, 2010.

[24] Mulet, J., M. Giudici, J. Javaloyes, and S. Balle. Square-wave switching by crossed-polarization gain modulation in vertical-cavity semiconductor lasers. *Phys. Rev. A* 76:043801, 2007.

[25] Gavrielides, A., D. W. Sukow, G. Burner, T. McLachlan, J. Miller, and J. Amonette. *Phys. Rev. E* 81:056209, 2010.

[26] Torre, M., A. Gavrieldies, and C. Masoller. Numerical characterization of transient polarization square-wave switching in two orthogonally coupled VCSELs. *Optics Express* 19:20269-20278, 2011.

[27] Masoller, C., D. Sukow, A. Gavrieldies, and M. Sciamanna. Bifurcation to square-wave switching in orthogonally delay-coupled semiconductor lasers: Theory and experiment. *Phys. Rev. A* 84:023838, 2011.

[28] Sciamanna, M., M. Virte, C. Masoller, and A. Gavrielides. Hopf bifurcation to square-wave switching in mutually coupled semiconductor lasers. *Phys Rev. E* 86:016218, 2012.

[29] Li, H., K. D. Choquette, A. Hohl, H. Hou, and A. Gavrielides. Stable polarization self-modulation in vertical-cavity surface-emitting lasers. *Appl. Phys. Lett.* 72:2355-2357, 1998.

[30] Lang, R., and K. Kobayashi. External Optical Feedback Effects on Semiconductor Injection Laser Properties. *IEEE J. of Quantum Electron.* QE-16:347-355, 1980.

[31] Martin-Regalado, J., N. B. Abraham, M. San Miguel, and F. Prati. Polarization Properties of Vertical-Cavity Surface-Emitting Lasers. *IEEE J. of Quantum Electron.* QE-33:765-783, 1997.

[32] San Miguel, M., Q. Feng, and J. V. Moloney. Light-polarization dynamics in surface emitting semiconductor lasers. *Phys. Rev. A* 52:1728-1739, 1995.